Theory and practice on the self-calibration of a rotating and zooming camera from two views

Y.Seo and K.S.Hong

Abstract: The paper deals with first the uniqueness of the self-calibration of a rotating and zooming camera, mathematically, given two views. It is assumed that the principal point and the aspect ratio are fixed but the focal length changes as the camera rotates. In this case, theoretically at least one inter-image homography is enough to compute the internal calibration parameters as well as the rotation, and the self-calibration is unique up to a rotation. Secondly, it is shown that the calibration parameters can be obtained through a linear computation, even though the original problem is highly nonlinear, when the principal point is given *a priori*. Finally, the authors analyse the effects of the deviation of the principal point on the linear computation of the focal lengths and the rotation. From the mathematical analysis, it is found that the more the camera changes its zoom the larger the effects are, and the larger the rotation angle the smaller the effects are. Thus, the image centre may be taken as the principal point in practical applications. Experimental results using real images are also given.

1 Introduction

This paper deals with the problem of self-calibration of a camera under pure rotation. Hartley proposed a method for a rotating camera of fixed internal calibration parameters by analysing the infinity homography that can be obtained from image matches [1]. However, the constraint of fixed calibration parameters is too restrictive since zooming and autofocusing are now usual. Agapito *et al.* proposed a nonlinear method [2], and a linear calibration method for a rotating and zooming camera [3]. Seo and Hong showed mathematically that, when skew is assumed zero, self-calibration of a zooming and rotating camera is possible and unique up to one rotation [4, 5]. They proposed an iterative estimation method. Hayman studied ambiguities and problems of applying self-calibration in Euclidean reconstruction from two independently rotating and zooming cameras [6].

The assumption of no translation has been adopted in the literature about the self-calibration of a rotating camera [1, 3, 5], even though this assumption can be hardly obeyed, but practically the displacement of the image matches caused by the translation of the camera is small enough when the camera displacement is very small compared with the distance to the 3-D scene.

Section 2 shows that one inter image homography (infinity homography) is sufficient for computing internal camera parameters when the aspect ratio and the principal point are fixed in time. We show theoretically that this calibration is unique up to a rotation which corresponds to the freedom in selecting the camera co-ordinate system.

However, the equation for computing the calibration parameters from the homography is highly nonlinear. Thus, we show that the computation of the calibration parameters from the inter-image homography can be done linearly when the principal point is known *a priori*. We also investigate the problem of degenerate camera rotations. Similar methods for the linear computation of the calibration parameters can be found in [3–5].

We also discuss the effect of the estimation error of the principal point on the estimation of the focal length and rotation matrix. Given the principal point, the self-calibration becomes a simple linear equation problem. Also, the principal point is practically around the image centre, which has been shown in the experiments of the earlier researchers [3, 4]. Then, what will happen if we take the image centre as the principal point? We analytically show that it will cause a small bias in the estimation of the focal lengths and rotation angle and direction.

Our analysis is also meaningful when we have an *a priori* estimate of the principal point since it may be obtained from the process of zooming the camera as in [7] and [8]. In these cases, too, we are concerned about the accuracy of the *a priori* estimation or its effect on the other parameters, in real applications. Our mathematical analysis and simulation using synthetic data give the effect of the principal point error, quantitatively, on our self-calibration algorithm. Finally, our algorithm is tested using real images.

This work is a development of the authors' previous work [5, 9].

2 Uniqueness of self-calibration

Every vector is denoted by a column vector. We represent an image point by $\boldsymbol{x} = [u, v, 1]^T$ and a 3-D point by $\boldsymbol{X} =$

IEE Proceedings online no. 20010078

DOI: 10.1049/ip-vis:20010078

Paper first received 2nd August 1999 and in revised form 12th October 2000

The authors are with the Department of Electronic & Electrical Engineering, Pohang University of Science and Technology (POSTECH), Pohang, Kyungbook, Republic of Korea, 790-784

$[X, Y, Z, 1]^T$. A 3-D point $\boldsymbol{X}$ projects to the image $\boldsymbol{x}$ through a perspective camera $\boldsymbol{P}$:

$$\boldsymbol{x} \sim \boldsymbol{PX} \tag{1}$$

where $\sim$ means the equality up to a non-zero scale. The 3×4 camera matrix $\boldsymbol{P}$ can be decomposed into calibration $\boldsymbol{K}$ and motion $\boldsymbol{R}$ and $\boldsymbol{t}$:

$$\boldsymbol{P} = \boldsymbol{K}[\boldsymbol{R} \mid \boldsymbol{t}] = [\tilde{\boldsymbol{P}} \mid \boldsymbol{0}] \tag{2}$$

where $\boldsymbol{t}$ is the translation vector and we may set $\boldsymbol{t}$ to zero since we are dealing with a pure rotating camera, and $\tilde{\boldsymbol{P}} \sim \boldsymbol{KR}$. In this paper, we consider a zero-skew calibration matrix $\boldsymbol{K}$:

$$\boldsymbol{K} = \begin{bmatrix} f\gamma & 0 & u_0 \\ & f & v_0 \\ & & 1 \end{bmatrix} \tag{3}$$

where (u_0, v_0) is the principal point, γ the aspect ratio, and f the effective focal length. We assume that (u_0, v_0) and γ do not change as the camera varies its zoom or focus.

Note that there exists a 2-D projective transformation $\boldsymbol{H}$, taking image $\mathcal{I}_0$ to image $\mathcal{I}_1$ ($\mathcal{I}_1 \sim \boldsymbol{H}\mathcal{I}_0$), whose matrix is of the form:

$$\boldsymbol{H} \sim \boldsymbol{K}_1 \boldsymbol{R}_1 \boldsymbol{K}_0^{-1} \tag{4}$$

where $\boldsymbol{R}_1$ is the rotation of the camera. The inter-image homography $\boldsymbol{H}$ can be computed from image matching pairs: $\boldsymbol{x}_1 \sim \boldsymbol{H}\boldsymbol{x}_0$. Using the homography $\boldsymbol{H}$, we may find the camera matrices $\tilde{\boldsymbol{P}}_0 = \boldsymbol{K}_0$ and $\tilde{\boldsymbol{P}}_1 = \boldsymbol{K}_1\boldsymbol{R}_1$ that satisfy the relationship $\boldsymbol{H} \sim \tilde{\boldsymbol{P}}_1 \tilde{\boldsymbol{P}}_0^{-1} \sim \boldsymbol{K}_1\boldsymbol{R}_1\boldsymbol{K}_0^{-1}$. However, note that given one such pair of camera matrices $(\tilde{\boldsymbol{P}}_0, \tilde{\boldsymbol{P}}_1)$, the pair $(\tilde{\boldsymbol{P}}_0\boldsymbol{Q}, \tilde{\boldsymbol{P}}_1\boldsymbol{Q})$ may also be a possible choice of camera matrices, where $\boldsymbol{Q}$ is a non-singular 3×3 matrix. Here we will show that $\boldsymbol{Q}$ is a rotation matrix.

2.1 The uniqueness

Denote by $\mathcal{M}_{zs}$ the manifold of all camera matrices that represent zero-skew cameras. Also, denote by $\mathcal{G}_{zs}$ the group of transformations that preserve the property in lemma 1, and the group of orthogonal transformations up to scale by $\mathcal{G}_O$:

$$\mathcal{G}_{zs} = \{\boldsymbol{Q} \in \mathcal{G}_{\mathcal{P}} \mid (\tilde{\boldsymbol{P}} \in \mathcal{M}_{zs}) \Rightarrow \tilde{\boldsymbol{P}}\boldsymbol{Q} \in \mathcal{M}_{zs}\}$$

$$\mathcal{G}_O = \{\lambda\boldsymbol{Q} \mid \boldsymbol{Q}\boldsymbol{Q}^T = \boldsymbol{I},\ 0 \neq \lambda \in \mathrm{R}\}$$

Lemma 1 ([10]): A camera matrix $\tilde{\boldsymbol{P}} = \boldsymbol{KR} = [\boldsymbol{p}_1, \boldsymbol{p}_2, \boldsymbol{p}_3]^T$ represents a zero-skew camera if and only if

$$(\boldsymbol{p}_1 \times \boldsymbol{p}_3) \cdot (\boldsymbol{p}_2 \times \boldsymbol{p}_3) = 0 \tag{5}$$

Proposition 1: The groups $\mathcal{G}_{zs}$ and $\mathcal{G}_O$ are equivalent, i.e.

$$\mathcal{G}_{zs} = \mathcal{G}_O$$

Proof: It is clear that $\mathcal{G}_O \subseteq \mathcal{G}_{zs}$. Now we show that $\mathcal{G}_O \supseteq \mathcal{G}_{zs}$. Assume that $\tilde{\boldsymbol{P}}$ represents a zero-skew camera, and $\boldsymbol{Q}$ is a projective transformation in $\mathcal{G}_{zs}$. Then, from the definition, $\tilde{\boldsymbol{P}}\boldsymbol{Q} = \boldsymbol{KRQ}$ can be rewritten in the form of $\boldsymbol{K}'\boldsymbol{R}'$ where $\boldsymbol{K}'$ is a zero-skew calibration matrix and $\boldsymbol{R}'$ is an orthogonal matrix. Also $\boldsymbol{UQV}$ has this property for every pair of orthogonal matrices $\boldsymbol{U}$ and $\boldsymbol{V}$, since

$$\boldsymbol{KRUQV} = \boldsymbol{KR}''\boldsymbol{QV} = \boldsymbol{K}'\boldsymbol{R}'''\boldsymbol{V} = \boldsymbol{K}'\boldsymbol{R}'$$

where $\boldsymbol{R}''$ and $\boldsymbol{R}'''$ denote orthogonal matrices. Now, using singular value decomposition of $\boldsymbol{Q}$ we may write

$$\boldsymbol{D} = \boldsymbol{UQV} = \mathrm{diag}(d_1, d_2, d_3) \tag{6}$$

Suppose that the rotation matrix $\boldsymbol{R}$ is given by

$$\boldsymbol{R} = \boldsymbol{R}_z(\psi)\boldsymbol{R}_y(\phi)\boldsymbol{R}_x(\theta) \tag{7}$$

where $\boldsymbol{R}_x$, $\boldsymbol{R}_y$, and $\boldsymbol{R}_z$ represent the rotation matrices for the x-, y-, and z-axes, respectively. According to lemma 1, $\boldsymbol{RD} = [\boldsymbol{a}_1, \boldsymbol{a}_2, \boldsymbol{a}_3]^T$ is a zero-skew calibration matrix if and only if $(\boldsymbol{a}_1 \times \boldsymbol{a}_3) \cdot (\boldsymbol{a}_2 \times \boldsymbol{a}_3) = 0$. After some calculations we have

$$\begin{aligned} &(\boldsymbol{a}_1 \times \boldsymbol{a}_3) \cdot (\boldsymbol{a}_2 \times \boldsymbol{a}_3) \\ &\quad = \cos^2\psi[d_1^2(d_2^2 - d_3^2)\cos\theta\sin\theta\sin\phi] \\ &\quad\quad - \sin^2\psi[d_1^2(d_2^2 - d_3^2)\cos\theta\sin\theta\sin\phi] \\ &\quad\quad - \frac{\sin 2\psi}{2}[d_1^2\sin^2\theta(d_2^2 - d_3^2\sin^2\phi) \\ &\quad\quad + d_1^2\cos^2\theta(d_3^2 - d_2^2\sin^2\phi) \\ &\quad\quad - d_2^2 d_3^2\cos^2\phi] \end{aligned} \tag{8}$$

That is, $\boldsymbol{RD}$ is a zero-skew calibration matrix is and only if $d_1 = d_2 = d_3$. Thus, all singular values of $\boldsymbol{Q}$ are equal, which means that $\boldsymbol{Q}$ is an orthogonal matrix. □

Remark 1: This proposition and proof may be regarded as a modified version of the theorem of Heyden and Åström [11], applied to a rotating and zooming camera.

Remark 2: Note that the matrix $\boldsymbol{Q}$ is related to the selection of the camera co-ordinate system. Therefore, choosing the origin of the camera co-ordinate system with respect to the reference image determines implicitly the matrix $\boldsymbol{Q}$.

3 Linear estimation method

This Section describes how to compute the calibration and rotation from the homography of image matches from two views. We show that, when the principle point is given *a priori*, we can compute the other parameters linearly by analysing the components of the inter-image homography.

3.1 Aspect ratio and focal lengths with known principal point

When the principal point (u_0, v_0) is known, we can eliminate it from the homography matrix $\boldsymbol{H}$ by multiplying $\boldsymbol{C}^{-1}$ to the left and $\boldsymbol{C}$ to the right

$$\boldsymbol{H}' = \boldsymbol{C}^{-1}\boldsymbol{HC} \tag{9}$$

where

$$\boldsymbol{C} = \begin{bmatrix} 1 & & u_0 \\ & 1 & v_0 \\ & & 1 \end{bmatrix} \tag{10}$$

Without loss of generality, we henceforth use the notation $\boldsymbol{H}$ instead of $\boldsymbol{H}'$ for the homography matrix from which the principal point has been removed. Then, eqn. 4 is rewritten as follows

$$\boldsymbol{H}\boldsymbol{K}_0\boldsymbol{K}_0^T\boldsymbol{H}^T \sim \boldsymbol{K}_1\boldsymbol{K}_1^T \tag{11}$$

and the calibration matrix $\boldsymbol{K}_i$ is of the form

$$\boldsymbol{K}_i = \mathrm{diag}(\gamma f_i, f_i, 1) \quad \text{for} \quad i = 0, 1 \tag{12}$$

Eqn. 11 then gives us three equations for $g_0^2 = (\gamma f_0)^2$ and f_0^2

$$\begin{bmatrix} h_{11}h_{21} & h_{12}h_{22} \\ h_{11}h_{31} & h_{12}h_{32} \\ h_{21}h_{31} & h_{22}h_{32} \end{bmatrix} \begin{bmatrix} g_0^2 \\ f_0^2 \end{bmatrix} = \begin{bmatrix} -h_{13}h_{23} \\ -h_{13}h_{33} \\ -h_{23}h_{33} \end{bmatrix} \tag{13}$$

After computing g_0 and f_0, we can compute γ and f_1 linearly

$$\gamma = \frac{g_0}{f_0} \tag{14}$$

$$f_1^2 = \frac{f_0^2 h_{21}^2 + (\gamma f_0)^2 h_{22}^2 + h_{23}^2}{f_0^2 h_{31}^2 + (\gamma f_0)^2 h_{32}^2 + h_{33}^2} = \frac{f_0^2 h_{11}^2 + (\gamma f_0)^2 h_{12}^2 + h_{13}^2}{f_0^2 h_{31}^2 + (\gamma f_0)^2 h_{32}^2 + h_{33}^2} \tag{15}$$

However, there are singular cases where the above computations cannot be applied. When the rotation is about the x-axis, the rotation matrix is of the form

$$\boldsymbol{R}_1 = \boldsymbol{R}_x(\theta) = \begin{bmatrix} 1 & & \\ & \cos\theta & -\sin\theta \\ & \sin\theta & \cos\theta \end{bmatrix} \tag{16}$$

when the rotation angle is θ. Then, due to this special form of the rotation matrix we have

$$\boldsymbol{R}_x(\theta) = \boldsymbol{D}_x(\lambda)\boldsymbol{R}_x(\theta)\boldsymbol{D}_x(\lambda^{-1}) \tag{17}$$

where $\boldsymbol{D}_x(\lambda) = \mathrm{diag}(\lambda, 1, 1)$. That is, there are multiple solutions for the calibration parameter g_0 that satisfy the equation $\boldsymbol{H} = \boldsymbol{K}_1\boldsymbol{R}_x\boldsymbol{K}_0^{-1}$. In the case of rotations about the y-axis, we come to have multiple solutions for f_0 and f_1 through the same reasoning. The singular motion problem was investigated previously in [1] for the fixed calibration model and extended to the time varying calibration models in [3, 4].

3.2 Focal length estimation with known principal point and aspect ratio

Now we assume that we have an *a priori* estimate of the aspect ratio together with the principal point. The calibration matrix has now the following form after removing the known factors γ and (u_0, v_0) from $\boldsymbol{K}_i$

$$\boldsymbol{K}_i = \mathrm{diag}(f_i, f_i, 1), \quad \text{for } i = 0, 1 \tag{18}$$

Then, we can rewrite eqn. 4 as

$$\boldsymbol{H}\boldsymbol{K}_0\boldsymbol{K}_0^{\mathrm{T}}\boldsymbol{H}^{\mathrm{T}} \sim \boldsymbol{K}_1\boldsymbol{K}_1^{\mathrm{T}}, \tag{19}$$

from which we have three equations to compute f_0:

$$f_0^2(h_{11}h_{21} + h_{12}h_{22}) = -h_{13}h_{23} \tag{20}$$

$$f_0^2(h_{11}h_{31} + h_{12}h_{32}) = -h_{13}h_{33} \tag{21}$$

$$f_0^2(h_{21}h_{31} + h_{22}h_{32}) = -h_{23}h_{33} \tag{22}$$

and two equations for f_1:

$$f_1^2 = \frac{f_0^2(h_{11}^2 + h_{12}^2) + h_{13}^2}{f_0^2(h_{31}^2 + h_{32}^2) + h_{33}^2} \tag{23}$$

$$f_1^2 = \frac{f_0^2(h_{21}^2 + h_{22}^2) + h_{23}^2}{f_0^2(h_{31}^2 + h_{32}^2) + h_{33}^2} \tag{24}$$

Note that the exact form $\bar{\boldsymbol{H}}$ of $\boldsymbol{H}$ in the case of the pure rotation about the x-axis is

$$\bar{\boldsymbol{H}} = \bar{\boldsymbol{K}}_1\boldsymbol{R}_x^{\theta}\bar{\boldsymbol{K}}_0 = \begin{bmatrix} f_1 f_0^{-1} & & \\ & \cos\theta f_1 f_0^{-1} & -\sin\theta f_1 \\ & \sin\theta f_0^{-1} & \cos\theta \end{bmatrix} \tag{25}$$

where θ is the rotation angle, and we have the following:

Remark 3: When the rotation is about the x-axis eqns. 20 and 21 are not valid in the computation of f_0, because they are identically zeros ($f_0 \cdot (0 + 0) = 0$). Only eqn. 22 must be used.

Remark 4: When the rotation is about the y-axis, only eqn. 21 is valid through the same reasoning.

Thus, our approach is to check the image motion direction using the matching points and choose eqn. 21 or eqn. 22 according to the average of the image motion directions.

3.3 Rotation estimation

The rotation matrix $\boldsymbol{R}_1$ can be written as

$$\boldsymbol{R}_1 = \frac{\boldsymbol{K}_1^{-1}\boldsymbol{H}\boldsymbol{K}_0}{\det(\boldsymbol{K}_1^{-1}\boldsymbol{H}\boldsymbol{K}_0)^{1/3}}. \tag{26}$$

In the estimation, we use Euler representation for the rotation matrix $\boldsymbol{R}$. After computing the singular value decomposition $\boldsymbol{U}\boldsymbol{D}\boldsymbol{V}^{\mathrm{T}}$ of $\boldsymbol{K}_1^{-1}\boldsymbol{H}\boldsymbol{K}_0$, we obtain an estimate $\hat{\boldsymbol{R}}$ by the following

$$\hat{\boldsymbol{R}} = \boldsymbol{U}\,\mathrm{diag}(1, 1, \det(\boldsymbol{U}\boldsymbol{V}^{\mathrm{T}}))\boldsymbol{V}^{\mathrm{T}} \tag{27}$$

which minimises $\| \hat{\boldsymbol{R}} - \boldsymbol{R}_1 \|_F$ where $\| \cdot \|_F$ denotes Frobenious norm, and compute the rotation axis $\hat{\boldsymbol{n}}$ and angle $\hat{\Omega}$ using the vector $\boldsymbol{a} = (r_{32} - r_{23}, r_{13} - r_{31}, r_{21} - r_{12})^{\mathrm{T}}$

$$\hat{\boldsymbol{n}} = \frac{\boldsymbol{a}}{\|\boldsymbol{a}\|} \tag{28}$$

$$\hat{\Omega} = \arctan2(\|\boldsymbol{a}\|, \mathrm{Tr}(\boldsymbol{R}) - 1) \tag{29}$$

where $\mathrm{Tr}(\boldsymbol{R})$ is the trace of $\boldsymbol{R}$ and r_{ij} is the (i, j)-th element of $\hat{\boldsymbol{R}}$, using the fact that

$$\|\boldsymbol{a}\| = 2\sin\Omega \tag{30}$$

$$\mathrm{Tr}(\boldsymbol{R}) = 1 + 2\cos\Omega \tag{31}$$

4 Locating the principal point

4.1 Mathematical analysis without image noise

Here we consider the effect of the deviation of the principal point. Since we do not know the exact principal point, the calibration matrices $\boldsymbol{K}_k$, $k = 0, 1$, will have some deviation from the truth

$$\tilde{\boldsymbol{K}}_k = \bar{\boldsymbol{K}}_k + \boldsymbol{K}_\Delta = \begin{bmatrix} f_k & & \\ & f_k & \\ & & 1 \end{bmatrix} + \begin{bmatrix} 0 & 0 & \Delta_x \\ 0 & 0 & \Delta_y \\ 0 & 0 & 0 \end{bmatrix} \tag{32}$$

Accordingly, the perturbed version $\tilde{\boldsymbol{H}} = \tilde{\boldsymbol{K}}_1\boldsymbol{R}_1\tilde{\boldsymbol{K}}_0^{-1}$ of $\tilde{\boldsymbol{H}}$ can be computed and decomposed into two parts, the truth term $\bar{\boldsymbol{H}}$ and the error term $\boldsymbol{H}_\Delta$:

$$\tilde{\boldsymbol{H}} = \bar{\boldsymbol{H}} + \boldsymbol{H}_\Delta \tag{33}$$

Without loss of generality, we assume the rotation matrix $\boldsymbol{R}_1$ is the composition of the rotations about the x-axis and y-axis:

$$\boldsymbol{R}_1 = \boldsymbol{R}_y(\theta_Y)\boldsymbol{R}_x(\theta_X) \tag{34}$$

Additionally, we assume that the rotation angle θ_X is larger than θ_Y. After some algebraic calculation, we have an approximation $\hat{f}_0$ through Taylor series expansion

$$\frac{\hat{f}_0^2}{f_0^2} \approx 1 + \frac{\Delta_y}{\tan\theta_X}\left(\frac{1}{f_0} - \frac{\cos\theta_Y}{f_1}\right) \tag{35}$$

Notice that this approximation depends only on Δ_y. We use eqn. 23, replacing f_0 with $\hat{f}_0$, for computing an estimate $\hat{f}_1$, and its approximation is given by

$$\frac{\hat{f}_1^2}{f_1^2} \approx 1 + \frac{\Delta_y}{\tan\theta_X}\left(\frac{1}{f_0} - \frac{\cos\theta_Y}{f_1}\right) - 2\cos^2\theta_Y \cos^2\theta_X\left(\frac{\Delta_y \tan\theta_X}{f_0} + \frac{\Delta_x \tan\theta_Y}{f_1}\right) \quad (36)$$

Remark 5: Eqns. 35 and 36 express that the more the focal length changes due to the zoom operation of the camera, the larger is the effect of the principal point error.
Remark 6: The larger the rotation angle is, the smaller the effect of the principal point error is.

For example, when $f_0 = 1000$, $f_1 = 900$, $\Delta_x = \Delta_y = 20$ pixel, $\theta_X = 3°$, and $\theta_Y = 0$, we have about 2.1% deviation in the estimations $\hat{f}_0$ and $\hat{f}_1$ from the true values.

As for the rotation $\boldsymbol{R}_1$, eqn. 26 gives the deviated rotation matrix when the estimated focal lengths are used. But, in this case, it is difficult to get an analytic solution. After estimating the rotation matrix, we now illustrate the extent of the deviation.

Now we present graphically the effects of the deviation of the principal point. The parameter values for the plots are: $f_0 = 1000$, $f_1 = 900$, $\theta_X = -5°$ and $\theta_Y = 0°$. Fig. 1 shows the plot of $(1 - \hat{f}_0/f_0)$. Notice that the maximum error is within 4% when $|\Delta_y| = 50$ pixel. Fig. 2 shows the graphs of $(1 - \hat{f}_1/f_1) \times 100\%$. Notice also that the maximum error is below 4%, even at the deviation of $\Delta_x = \Delta_y = 50$ pixel. Fig. 3 shows error plots for the rotation angle and direction caused by the principal point error. The error for the rotation angle was maximally below 0.2° at $\Delta_x = \Delta_y = 50$ pixel, as shown in Fig. 3*a*. We computed the angle $\psi = \cos^{-1}(\bar{\boldsymbol{n}} \cdot \hat{\boldsymbol{n}})$ between the true direction vector $\bar{\boldsymbol{n}}$ and estimated vector $\hat{\boldsymbol{n}}$, which was below 2.5° at maximum as shown in Fig. 3*b*.

4.2 Simulation with image noise

Now, we investigate the effect of the principal point error using two sets of parameters for synthetic image data. The parameters are shown in Table 1.

We generated randomly two sets of image data corresponding to two images and added Gaussian noise of standard deviation σ (pixels) to the coordinates of the synthetic data independently. We repeated 100 computations at each input noise level and plotted the average and standard deviation of each of the calibration parameters (focal lengths and rotation angles). Thus, the axes of abscissae of the plots correspond to the input noise level.

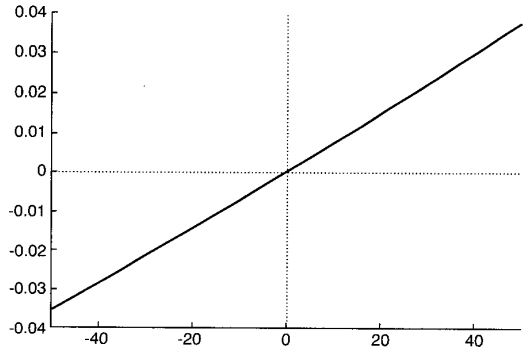

Fig. 1 *Error plot for* $(1 - \hat{f}_0/f_0)$ *against* Δ_y
For $f_0 = 1000$, $f_1 = 900$, $\theta_X = -5°$, and $\theta_Y = 0°$, the maximum of $(1 - \hat{f}_0/f_0)$ was within 0.04 – just 4% deviation at $\Delta y = 50$ pixel error

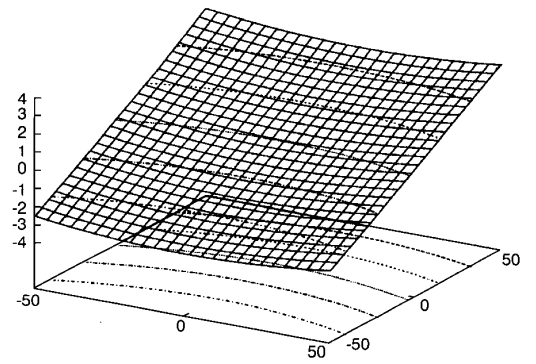

Fig. 2 *Error plot for* $(1 - \hat{f}_1/f_1) \times 100\%$
The maximum was below 4% at $\Delta_x = \Delta_y = 50$ pixel
—— 3
– – – 2.65
– · – · 1.5
· · · · 0.354
– · – · −0.792
– · · – · · −1.94

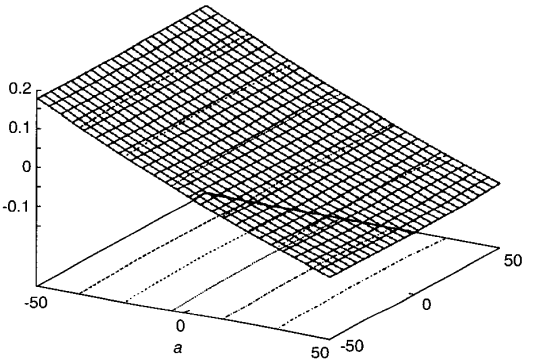

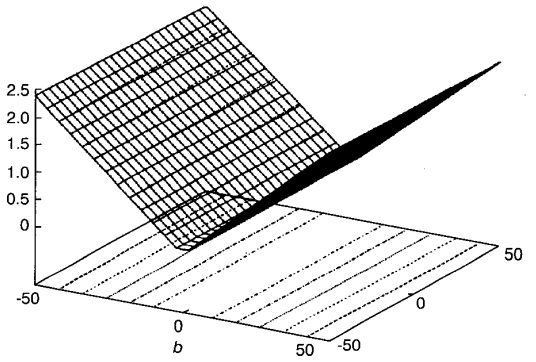

Fig. 3 *Error plots for rotation angle and axis*
a Rotation angle error
—— 3
– – – 0.124
– · – · 0.0705
· · · · 0.0168
– · – · −0.0369
– · · – · · −0.0906
b Rotation axis error
—— 3
– – – 2.01
– · – · 1.63
· · · · 1.24
– · – · 0.859
– · · – · · −0.476

Table 1: Two parameter sets for simulations

f_0	f_1	θ_X	θ_Y	θ_Z
1000	980	8°	6°	0°
1000	900	3°	2°	0.2°

There are five graphs in a plot, one of which corresponds to the case when we know the exact principal point ($u_0 = 320$, $v_0 = 240$ or $\Delta_x = \Delta_y = 0$) and the other four cases when we have a deviation in the principal point ($\Delta_x = \pm 20$ pixel, $\Delta_y = \pm 20$ pixel).

Fig. 4 shows the result for the first parameter set. Notice that the average values of f_0 are similar in Fig. 4*a*, seeming to be independent of the deviations in the principal point. This is because the zoom factor is not large enough ($1000 \rightarrow 980$) to yield the effect of the principal point error (Remark 5). Eqn. 35 gives about 0.8% bias from the truth, when $\Delta_y = 20$ pixel. Fig. 4*b* shows the plot for standard deviations, and we find that whatever the principal point error is, the standard deviations are almost the same. We can find similar results for the other parameters in Fig. 4.

In the experiments of Fig. 5, the focal length changed largely ($1000 \rightarrow 900$) and the rotation angles were relatively small. The effect of the principal point error can be seen easily. However, the plots of standard deviations still do not show any dependency on the deviation of the principal point. In contrast with the standard deviations, the plots of average values show a little dependency. Fig. 5*a* shows some biases in the average values of f_0 – about $[(1000 - 980)/1000] \times 100\% = 2\%$ bias down from the true value when $\Delta_y = +20$ pixel and a similar bias up when $\Delta_y = -20$ pixel. Fig. 5*c* shows average values of f_1 and illustrates about $(|900 - 922|/900) \times 100\% = 2.4\%$ biases in the same fashion. Notice that these biases were already expected from eqns. 35 and 36. Fig. 5*e* shows about 0.08° biases up and down for each of the rotation angles. Notice that, when input noise σ is larger than about 0.4 pixel, each of the biases is within one standard deviation range of its truth value.

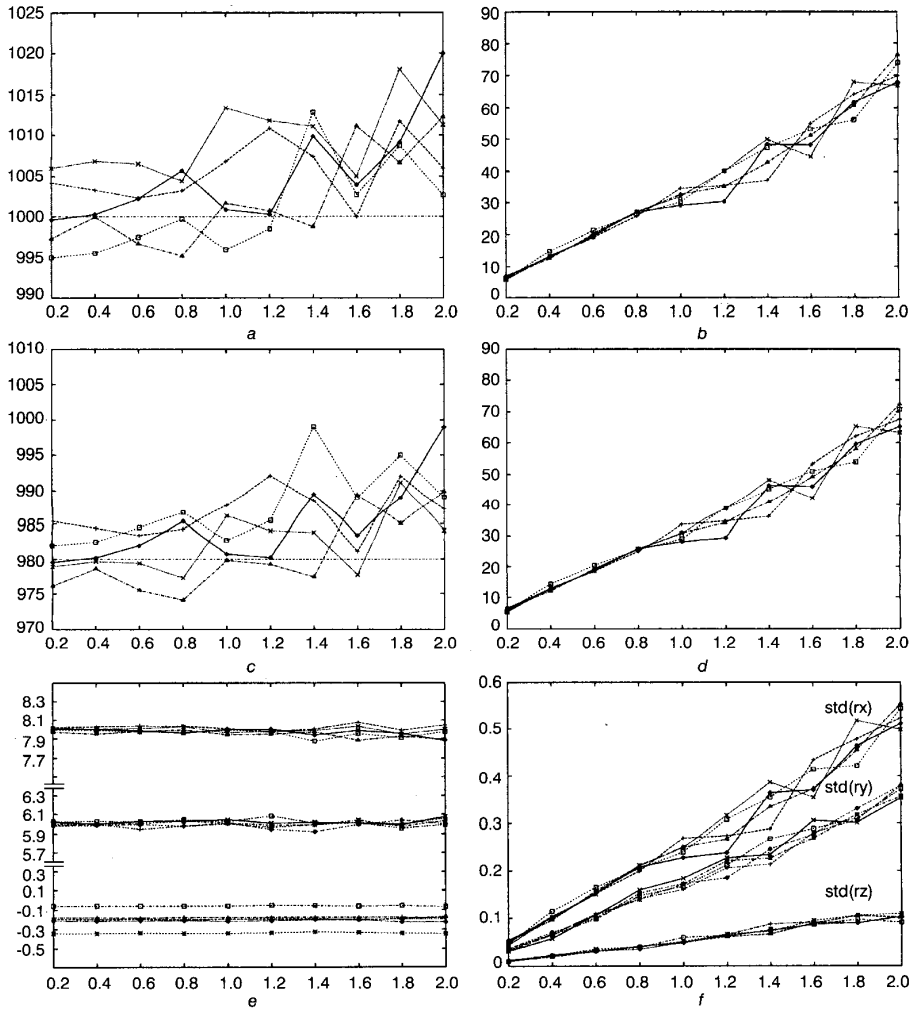

Fig. 4 *Simulation 1 ($f_0 = 1000, f_1 = 980, \theta_X = 8°, \theta_Y = 6°$)*

Plots of average and standard deviation corresponding to each of the five deviations in the principal point
a Mean of f_0
b Standard deviation of f_0
c Mean of f_1
d Standard deviation of f_1
e Mean of θ
f Standard deviation of θ

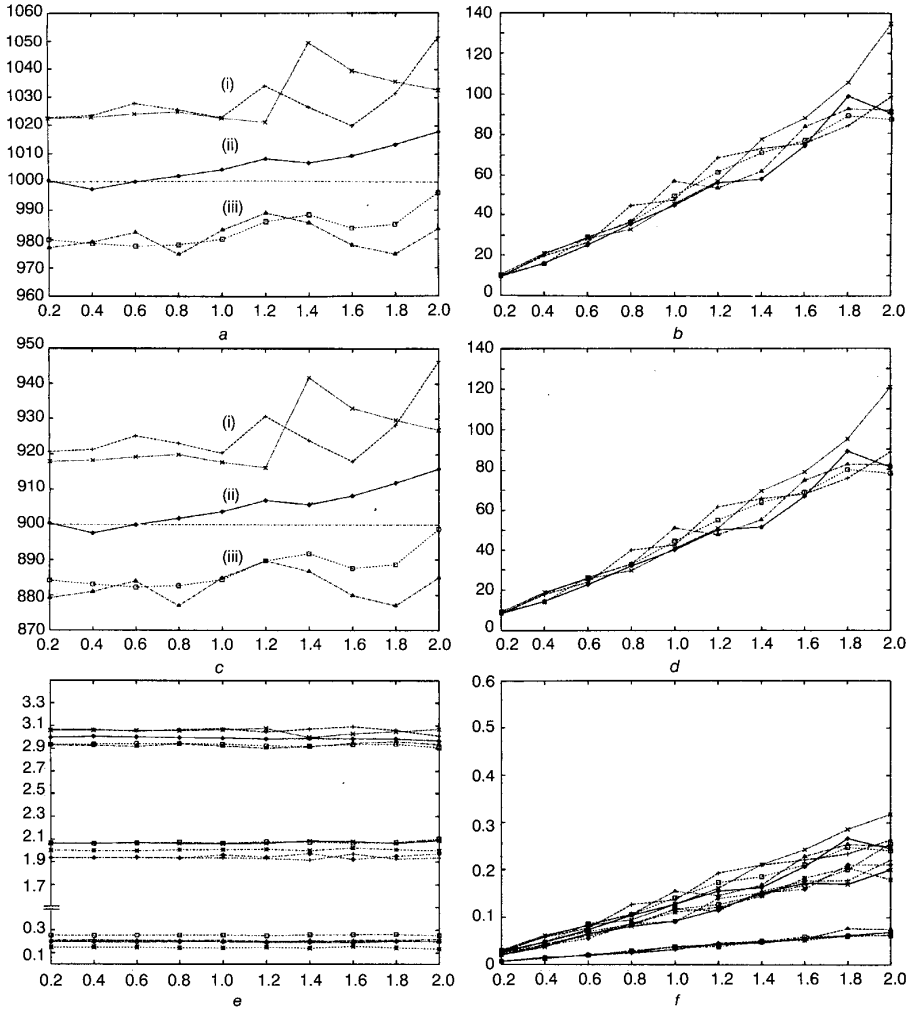

Fig. 5 *Simulation 2 ($f_0 = 1000, f_1 = 900, \theta_X = 3°, \theta_Y = 2°, \theta_Z = 0.2°$)*

About 2% biases were observed for the average values of f_0 and f_1, depending on the deviations in *a* and *c*. For the rotation angles, biases are about 0.08° in *e*. In contrast, the standard deviations do not show any dependencies, as shown in plots *b*, *d* and *f*.

a Mean of f_0
b Standard deviation of f_0
c Mean of f_1
d Standard deviation of f_1
e Mean of θ
f Standard deviation of θ

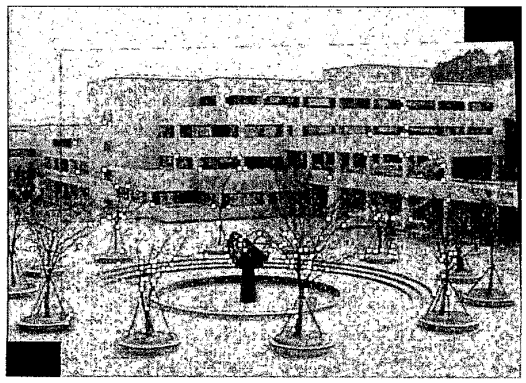

Fig. 6 *Experiment 1*

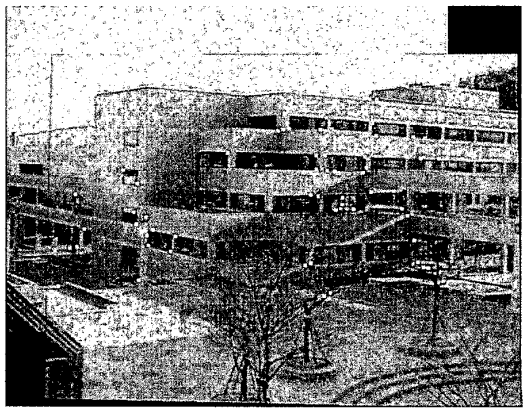

Fig. 7 *Experiment 2*

5 Real experiments

Fig. 6 shows a mosaic of two images obtained from a rotating camera on a tripod. As possible, the zoom was kept unchanged. The white points are the image matches which were used for estimating the homography. The estimate of the input noise variance is $(\hat{\sigma})^2 = (0.42 \text{ pixel})^2$. The result of the optimisation method of [4] gave estimates of the calibration parameters: $(u_0, v_0) = (324, 232.8)$, $\hat{f}_0 = 1160.3$, $\hat{f}_1 = 1158.7$ and the rotation angles $(-2.69°, 3.36°, -0.73°)$. When the principal point was set to the image centre, the result was: $\hat{f}_0 = 1161.7$, $\hat{f}_1 = 1164.0$ and $(-2.69°, 3.37°, -0.72°)$. Notice that we have almost the same calibration result.

In the next experiment, we changed the zoom factor of the camera. Fig. 7 is the mosaic image. The estimated input noise level was $(\hat{\sigma})^2 = (0.455 \text{ pixel})^2$. The optimisation algorithm gave the calibration result: $(u_0, v_0) = (317.8, 239.2)$, $\hat{f}_0 = 1259.0$, $\hat{f}_1 = 1186.1$ and $(-3.84°, 3.35°, 0.46°)$. At this time the zoom was $f_1/f_0 = 0.94$. When the principal point was set to the image centre, the result was: $\hat{f}_0 = 1259.3$, $f_1 = 1188.4$ and $(-3.84°, 3.35°, 0.46°)$. Notice that the estimated principal point of the optimisation method is close to the image centre (320, 240), and thus the two results shows almost the same values.

6 Conclusion

The first part of this paper shows that the self-calibration of a rotating and zooming camera, skew being assumed zero, is unique up to a rotation matrix which corresponds to the freedom of selecting the origin of the camera coordinate system. Next, it is shown that the nonlinear equations for the computation of the calibration parameters can be turned into linear equations when the principal point is given.

Then, studied is the effects of the principal point error, when an *a priori* estimate of the principal point is given, on the linear computation of the focal lengths and the rotation angles and direction. A mathematical analysis and results from the simulation using synthetic image data are presented.

This study is a prerequisite for further applications of the technique of self-calibration of a rotating and zooming camera. Particularly, we are usually confronted with rotating and zooming cameras in sports.

7 Acknowledgment

This work is partially supported by Korea Science and Engineering Foundation (KOSEF). Yongduek Seo thanks professor Kenichi Kanatani of Gunma University, Japan, for the free C++ source program to compute inter-image homographies optimally.

8 References

1 HARTLEY, R.I.: 'Self calibration of stationary cameras', *Int. J. Comput. Vis.*, 1997, **22**, (1), pp. 5–23
2 AGAPITO, L., HAYMAN, E., and REID, I.: 'Self-calibration of a rotating camera with varying intrinsic parameters'. Proceedings of British *Machine Vision* Conference, 1998, pp. 105–114
3 AGAPITO, L., HAYMAN, E., and REID, I.: 'Linear calibration of a rotating and zooming camera'. Proceedings of IEEE Conference *Computer Vision and Pattern Recognition*, 1999
4 SEO, Y.D., and HONG, K.S.: 'Autocalibration of a rotating and zooming camera'. Proceedings of IAPR Workshop on *Machine Vision Applications*, 1998, pp. 274–277
5 SEO, Y.D., and HONG, K.S.: 'About the self-calibration of a rotating and zooming camera: Theory and practice'. Presented at IEEE International Conference on *Computer Vision*, 1999, Kerkyra, Greece
6 HAYMAN, E., AGAPITO, L., REID, I., and MURRAY, D.W.: 'The role of self-calibration in Euclidean reconstruction from two rotating and zooming cameras'. Proceedings of European Conference on *Computer Vision*, 2000, pp. 477–492
7 POLLEFEYS, M., VAN GOOL, L., and PROESMANS, M.: 'Euclidean 3d reconstruction from image sequences with variable focal lengths'. Proceedings of European Conference on *Computer Vision*, Cambridge, UK, 1996, pp. 31–42
8 PARK, S.-W., SEO, Y.D., and HONG, K.S.: 'Real-time camera calibration for virtual studio', *J. Real-Time Imaging*, 2000, **6**, (6), pp. 433–448
9 SEO, Y.D.: 'Non-metric augmented reality and flexible self-calibration'. PhD dissertation, Department of EE., Pohang University of Science and Technology (POSTECH), 2000
10 FAUGERAS, O.: 'Three-Dimensional Computer Vision' (MIT Press, Cambridge, 1993)
11 HEYDEN, A., and ÅSTRÖM, K.: 'Minimal conditions on intrinsic parameters for Euclidean reconstruction'. Presented at 2nd Asian Conference on *Computer Vision*, 1998, Hong Kong, China